

Neurophotonics

Neurophotonics.SPIEDigitalLibrary.org

Overexpression of channelrhodopsin-2 interferes with the GABA_B receptor-mediated depression of GABA release from the somatostatin-containing interneurons of the prefrontal cortex

Lei Liu
Wataru Ito
Alexei Morozov

Overexpression of channelrhodopsin-2 interferes with the GABA_B receptor-mediated depression of GABA release from the somatostatin-containing interneurons of the prefrontal cortex

Lei Liu,^a Wataru Ito,^a and Alexei Morozov^{a,b,c,*}

^aVirginia Tech Carilion Research Institute, Roanoke, Virginia, United States

^bVirginia Tech, School of Biomedical Engineering and Sciences, Blacksburg, Virginia, United States

^cVirginia Tech Carilion School of Medicine, Department of Psychiatry and Behavioral Medicine, Roanoke, Virginia, United States

Abstract. Region and cell-type restricted expression of light-activated ion channels is the indispensable tool to study properties of synapses in specific circuits and to monitor synaptic alterations by various stimuli including neuromodulators and behaviors, both *ex vivo* and *in vivo*. These analyses require the light-activated proteins or viral vectors for their delivery that do not interfere with the phenomenon under study. Here, we report a case of such interference in which the high-level expression of channelrhodopsin-2 introduced in the somatostatin-positive GABAergic neurons of the dorsomedial prefrontal cortex by an adeno-associated virus vector weakens the presynaptic GABA_B receptor-mediated suppression of GABA release. © 2018 Society of Photo-Optical Instrumentation Engineers (SPIE) [DOI: 10.1117/1.NPh.5.2.025003]

Keywords: channelrhodopsin 2; artifact; GABA_B receptor; presynaptic release; somatostatin interneurons.

Paper 17107LRR received Jul. 18, 2017; accepted for publication Feb. 5, 2018; published online Mar. 1, 2018.

1 Introduction

In circuit analyses, channelrhodopsin-2 (ChR2) and its analogue opsins have been used to identify long-range synaptic connections,¹ to compare strength of synapses among distinct classes of neurons within local microcircuits,² to study plastic changes elicited by neuromodulators,³ behavioral experience,^{4–6} and genetic mutations.^{7,8} Meanwhile, alterations of neuronal morphology and membrane properties had been reported in both excitatory and inhibitory neuronal opsins when expressed at high levels.^{9–11} While morphological analysis can provide a measure to determine the “healthy” levels of opsin-expressing neurons, the neuronal properties can become altered even in morphologically normal neurons. For example, presynaptically expressed ChR2 increases the release probability of neurotransmitter from glutamatergic synapses¹² and alters the dynamics of synaptic depression during high frequency stimulation,¹³ whereas Arch modulates the release of GABA.^{14,15} Despite such reports, the information about interferences by opsins with specific neuronal functions remains scarce, particularly with synaptic plasticity in distinct neuronal classes. Yet, such information is necessary for planning experiments on the functional interrogation of neuronal circuits.

One form of short-term synaptic plasticity is the depression of GABA release from GABAergic terminals that undergo repeated stimulation. The GABA_B autoreceptors at the terminals mediate that depression, which serves as a feedback control over GABAergic transmission.^{16–18} In the insular and somatosensory cortex of the rat brain, such depression is particularly pronounced when the interval between stimuli is around 200 ms.^{19,20} Recently, we have shown that in brain slices from the mouse

dorsomedial prefrontal cortex (dmPFC), GABA release from the somatostatin-positive GABAergic neurons (SOM-INs) expressing ChR2 undergoes strong presynaptic GABA_B receptor-mediated depression during their stimulation with the 5-Hz frequency train of blue light pulses.⁶ Here, we compared the GABA depression between two groups of slices prepared from the brains transduced with different amounts of adeno-associated virus vector (AAV) expressing ChR2 and found that the higher ChR2 expression diminished the GABA_B receptor-mediated depression of GABA release from SOM-IN of dmPFC.

2 Materials and Methods

2.1 Animals and Surgeries

C57BL/6N wild-type males or homozygous Gt(ROSA)26Sortm14(CAG-tdTomato)Hze/J males (Jackson stock 007908), backcrossed on C57BL/6N background for over six generations, were crossed with homozygous 129SvEv somatostatin interneurons-specific Cre-driver females Sst^{tm2.1(cre)Zjh}²¹ to obtain heterozygous Sst^{tm2.1(cre)Zjh} mice or double transgenics of the Sst^{tm2.1(cre)Zjh} and Gt(ROSA)26Sortm14(CAG-tdTomato)Hze alleles, which expressed tdTomato in the SOM-INs. The ChR2-AAV serotype 2 virus containing Cre-activated ChR2 gene [made from a plasmid pAAV-EF1a-double floxed-hChR2 (H134R)-EYFP (Addgene #20298)] and the GFP-AAV serotype 2 virus expressing GFP [made from a plasmid rAAV-hSyn-eGFP (Addgene #50465)] were obtained from the University of North Carolina Gene Therapy Vector Core (Chapel Hill, North Carolina). The male progeny at p21–p30 was injected into dmPFC in each hemisphere at 1.3 mm anterior, 0.4 mm

*Address all correspondence to: Alexei Morozov, E-mail: alexeim@vtc.vt.edu

lateral from the bregma, and 1.3 mm ventral from brain surface with 0.5 μ l of the viral solution containing 1×10^8 or 5×10^8 viral particles of the ChR2-AAV or a mixture of the ChR2-AAV and GFP-AAV (1×10^8 and 4×10^8 particles, respectively), as described.⁵ All experiments were approved by Virginia Tech IACUC and followed the NIH Guide for the Care and Use of Laboratory Animals.

2.2 Electrophysiology

Slice preparation and recordings were performed as described in Ref. 6. Coronal dmPFC slices, 300 μ m thickness, were prepared from p60-75 mice using DSK Microslicer (Ted Pella, Redding, California) and ice cold cutting solution contained (in mM) 110 choline Cl, 2.5 KCl, 1.2 NaH₂PO₄, 2.5 NaHCO₃, 20 glucose, 0.5 CaCl₂, and 5 MgSO₄, bubbled with a 95% O₂/5% CO₂. Before recording, slices were incubated at least 1 h at room temperature in (in mM) 120 NaCl, 3.3 KCl, 1.0 NaH₂PO₄, 25 NaHCO₃, 10 glucose, 0.5 CaCl₂, and 5 MgSO₄, bubbled with 95% O₂/5% CO₂. Recording chamber was superfused at 2 ml/min with (mM) 120 NaCl, 3.3 KCl, 1.0 NaH₂PO₄, 25 NaHCO₃, 10 glucose, 2 CaCl₂, and 1 MgCl₂, equilibrated with 95% O₂/5% CO₂. Whole cell recordings were obtained at 30°C \pm 1°C with Multiclamp 700B amplifier and Digidata 1440A (Molecular Devices, Sunnyvale, California). Recordings were performed from the dmPFC region located within +1.9 to +1.3 mm from bregma and 0.5 to 1.5 mm below the brain surface, which includes the prelimbic and anterior cingulate areas. Putative layer versus principal neurons (PNs) were identified by their pyramidal morphology under the Dodt gradient contrast optics (custom made) at 850-nm LED illumination (Thorlabs, Newton, New Jersey). SOM-INs were identified by red fluorescence. The 4 to 6 M Ω recording pipettes were filled, for inhibitory postsynaptic current (IPSC) measurement in PNs, with (in mM): 120 Cs-methanesulfonate, 5 NaCl, 1 MgCl₂, 10 HEPES, 0.2 EGTA, 2 ATP-Mg, 0.1 GTP-Na, 5 QX314, and, for recordings from SOM-INs, with (in mM) 120 K-gluconate, 5 NaCl, 1 MgCl₂, 10 HEPES, and 0.2 EGTA, 2 ATP-Mg, 0.1 GTP-Na, pH 7.3, osmolarity 285 Osm. Series resistance (R_s) was 10 to 20 M Ω and monitored throughout experiments. Data were not included in the analysis if R_s changed more than 20%. All membrane potentials were corrected for the junction potential of 12 mV. Light pulses (470 nm, 1 ms, or 200 ms for IPSC or photocurrent recordings, respectively) were generated using an LED lamp (Thorlabs) and a custom LED driver based on MOSFET and were delivered through a 40 \times objective lens (Olympus, Center Valley, Pennsylvania) at 0.56 to 23.5 mW/mm², calibrated by a photodiode power sensor (Thorlabs) at the tip of the lens. In most experiments, data from each cell were obtained from 19 to 20 stimuli sweeps separated by 20 s intervals. CGP52432 was from Tocris (Bristol, United Kingdom) and remaining chemicals were from Sigma-Aldrich (St. Louis, Missouri).

2.3 Data Analysis

Hyperpolarizing current steps were used to determine the membrane input resistance, which was calculated as the quotient of the voltage deflection divided by the value of the first current step (−100 pA). The membrane time constant was obtained using Clampfit software (Molecular Devices, Sunnyvale, California) from single exponential fits of transient decay curves from 5-mV voltage steps. To determine the spike

accommodation, a 750 ms 60 pA depolarizing current was injected to elicit spikes and the time intervals between the last and the second to the last spikes were divided by the interval between the first and the third spikes. Photocurrents were measured at the end of the 200-ms light pulses. Data from each neuron were taken as independent data points for statistical analyses. The numbers of patched cells and animals in each experiment are listed in figure legends. Statistical analyses were performed using GraphPad Prism (GraphPad Software, La Jolla, California) and StatView (SAS Institute, Cary, North Carolina). Differences were tested using the two-tailed paired and unpaired *t*-test. One- two- and three-way repeated measures ANOVA was used in the analyses of IPSC accommodation along repeated stimulation with 5-Hz light pulses with the time, virus titer, and CGP52432 as the factors.

3 Results

The short-term plasticity of GABAergic synapses formed by the SOM-INs on the layer versus PNs was examined by recording IPSCs evoked in the PNs voltage-clamped at 0 mV. The IPSCs were evoked by stimulating SOM-INs expressing ChR2-YFP with five pulses of blue light at 5-Hz frequency. [Figs. 1(a) and 1(c)]. At first, the irradiance was adjusted to obtain maximum IPSC responses (averages of 6.2 mW/mm² for the “high” and 7.1 mW/mm² for the “low virus” groups) and a comparison was made between slices expressing “high” and “low” levels of ChR2-YFP, which were obtained from animals transduced with 1×10^8 (low virus) and 5×10^8 (high virus) viral particles per hemisphere. The examples of ChR2-YFP fluorescence in dmPFC of animals transduced with the two levels of virus are shown in Fig. 1(b).

To examine the role of the GABA_B receptor in the synaptic plasticity, IPSCs were recorded first in ACSF without drugs and then, after 10 min perfusion with 10 μ M of CGP52432, a GABA_B receptor blocker. The IPSC data from the low virus slices are a part of an earlier publication⁶ but are included here to allow for the comparison between the high and low virus conditions.

The IPSC amplitudes decreased along the train in both the low and the high virus groups [low virus: $F(4, 10) = 121$, $p < 0.0001$; high virus: $F(4, 9) = 82$, $p < 0.0001$], but the decreases in the low virus group were greater [“train” * “level of virus” interaction, $F(1, 19) = 17.4$, $p < 0.0001$; Fig. 1(e)]. CGP52432 did not alter the amplitudes of IPSCs evoked by the first pulse in the train [Fig. 1(d)], but attenuated the IPSC depression in both groups (“train” * CGP52432 interaction, low virus: $F(1, 20) = 39.4$, $p < 0.0001$; high virus: $F(1, 18) = 11.0$, $p < 0.0001$). The attenuation was greater in the low virus group (“train” * CGP52432 * “level of virus” interaction: $F(2, 38) = 6.23$, $p = 0.0001$). Furthermore, CGP52432 eliminated the differences in IPSC attenuation along the train between the low and high virus groups [$F(1, 19) = 2.48$, $p > 0.05$]. Together, the data indicate that the GABA_B receptor signaling is mainly responsible for the differences in IPSC depression between the high and low virus groups.

The effects of “high virus” on IPSC dynamics could arise from the toxicity of high viral load, but not from ChR2 expression per se. To examine that possibility, mice were transduced with the mixture 1×10^8 virions of the ChR2-AAV and 4×10^8 virions of the GFP-AAV of the same serotype, called here the “low ChR2” group. The group replicated the “low virus” condition for the ChR2-AAV and the “high virus” condition

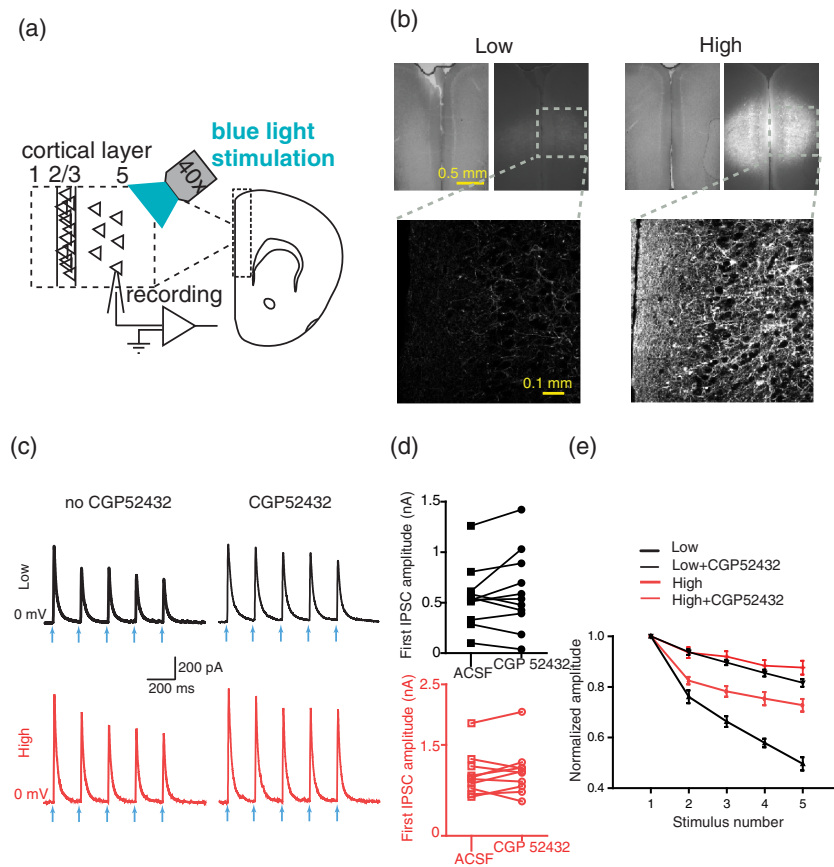


Fig. 1 ChR2 attenuates GABA_BR-mediated depression of GABA release. (a) Experimental scheme. Blue light stimulation of dmPFC and recording from layer versus PNs are illustrated. (b) dmPFC slices expressing ChR2-YFP in SOM-INs transduced with the low (low) and high (high) amounts of AAV with ChR2-YFP gene. Upper: visible (left) and yellow fluorescence (right) images of the same slices. Lower: confocal images of the areas marked with dashed squares. Several neurons in the high AAV group show accumulation of ChR2-YFP in the soma. (c) Examples of IPSCs evoked in layer versus PNs by 5-Hz train of blue light stimulation of SOM-interneurons expressing ChR2 before and after perfusion with CGP52432 (10 μM), averages of five sweeps are shown. The light pulses are indicated by blue arrows. (d) Amplitudes of the first IPSCs in the train before and after perfusion with CGP52432, lines connect data points representing the same cells. (e) IPSCs amplitudes normalized to the values of the first IPSC, before and after perfusion with CGP52432. Black and red colors represent slices with low ($n = 11$ cells, 3 mice) and high ($n = 10$ cells, 3 mice) levels of viral transduction. Data are presented as means \pm SEM.

for the total viral load and was compared with the “high ChR2” group of mice transduced with 5×10^8 virions of the ChR2-expressing AAV as in Fig. 1. The mice contained a Cre-activated tdTomato reporter to allow for visualization of the SOM-INs during whole cell recordings. In the high ChR2 group, some SOM-INs exhibited accumulation of ChR2-YFP in the soma and their plasma membrane did not form a gigaseal (data not shown), likely because of the toxicity of ChR2 at high levels of expression,¹⁰ so we did not record from such cells.

The IPSCs in PNs were evoked by five pulses of blue light at 5-Hz frequency. Five levels of irradiance ranging from 0.56 mW/mm², which was the threshold for evoking photocurrents in SOM-INs and IPSCs in PNs, to 23.5 mW/mm², were used in each recording. For the each level of irradiance, the IPSC declines along the train were significantly bigger in the “low ChR2” than in the “high ChR2” group [“train” * “level of virus” interaction; 0.56 mW/mm²: $F(1, 17) = 6.0$, $p = 0.0003$; 1.74 mW/mm²: $F(1, 17) = 4.4$; $p = 0.032$; 4.71 mW/mm²: $F(1, 17) = 3.4$, $p = 0.014$; 9.1 mW/mm²:

$F(1, 17) = 3.9$, $p = 0.007$; 23.5 mW/mm²: $F(1, 17) = 3.3$, $p = 0.015$; Figs. 2(a)–2(f)]. To test whether the smaller IPSC amplitude in the “low ChR2” group contributes the bigger IPSC declines, we compared the two groups under the conditions when the first IPSCs in the train had similar amplitudes in the “high ChR2” and “low ChR2” slices (876 ± 159 pA at 0.56 mW/mm² / “high ChR2” versus 949 ± 170 pA at 4.71 mW/mm² / “low ChR2”). Notably, the IPSC declines along the train in the “low ChR2” group remained bigger [“train” * “level of virus” interaction; $F(1, 17) = 2.7$, $p = 0.03$; Fig. 2(b)–red versus 2(d)–black].

To test effects of ChR2 expression on SOM-INs’ intrinsic properties, we performed whole cell recordings from these cells identified by the tdTomato red fluorescence [Fig. 2(g)]. Light-evoked depolarizing currents were recorded from all patched cells, indicating a 100% transduction of the ChR2-AAV. The “high ChR2” SOM-INs exhibited the photocurrents of larger amplitudes [Fig. 2(h)] but did not differ in the input resistance, membrane time constant, excitability, and spike accommodation from the “low ChR2” cells [Fig. 2(i)].

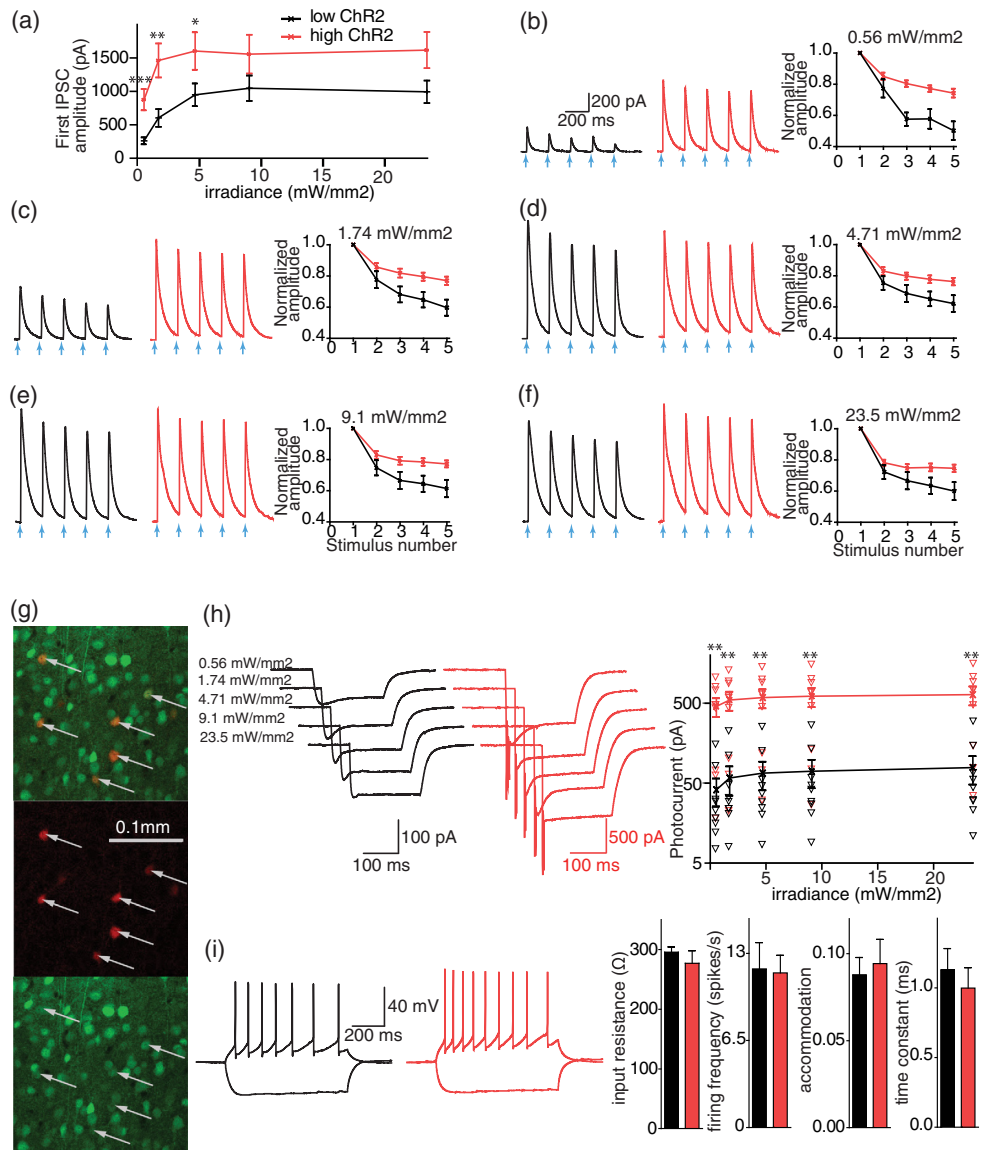


Fig. 2 Under the same viral load, ChR2 attenuates IPSC accommodation at all levels of light stimulation but it does not change the membrane and firing properties of SOM-INs. (a)–(f) Voltage clamp recordings from PN in the “low ChR2” and “high ChR2” groups. (a) Mean amplitudes of the first IPSCs in the 5-Hz trains as a function of irradiance. (b)–(f) IPSCs evoked in layer versus PN by 5-Hz trains of blue light pulses at five irradiances indicated in each panel. Left two traces: IPSC examples showing averages of five sweeps from the low ChR2 (left) and high ChR2 (right) groups. Light pulses are indicated by blue arrows. Right: IPSCs amplitudes normalized to the values of the first IPSC. Black and red colors represent the “low ChR2” ($n = 11$ cells, 3 mice) and “high ChR2” ($n = 8$ cells, 3 mice) groups. (g) A confocal image of dmPFC layer 5 in the slice from a SOM-Cre/tomato-reporter double transgenic mouse of the “low ChR2” group. The SOM-INs (arrows) are identified by red fluorescence; the green fluorescence results from the AAV2-hSyn-eGFP transduction. (h)–(i) Recordings from SOM-INs. (h) Photocurrents elicited in SOM-INs by the 200-ms pulses of blue light at the indicated irradiances. Left two sweeps: examples of traces from the low ChR2 (left, black) and high ChR2 (right, red) groups. Right graph: summary diagram for the steady state amplitudes, logarithmic Y-axis. Means, SEM, and values for each neuron are shown. (i) Intrinsic properties of SOM-INs. Left two sweeps: examples of membrane potentials upon injecting depolarizing (+60 pA) and hyperpolarizing (−100 pA) current steps in SOM-INs (black: the low ChR2 and red: the high ChR2 group). Right: summary diagrams for input resistance, firing frequency, spike accommodation and membrane time constant. Black and red colors represent “low ChR2” ($n = 9$ cells, 3 mice) and “high ChR2” ($n = 9$ cells, 3 mice) groups. Data are presented as means \pm SEM. * $p < 0.05$, ** $p < 0.01$, *** $p < 0.001$.

4 Discussion

The key finding here is that with the higher expression of ChR2 in SOM-INs, the light-induced GABA release from these cells is less susceptible to the GABA_B-mediated depression.

Our observation of an attenuated IPSC accommodation with the higher amounts of the ChR2-expressing virus could be explained by several mechanisms: (1) a general toxicity of a higher titer AAV vector, independent of ChR2, (2) effects of

ChR2 on the membrane properties on SOM-INs that determine their firing, and (3) a counteracting effect of photocurrents on the inhibition of GABA release. The effects of the general AAV toxicity on IPSC accommodation were ruled out by equalizing the total viral titers between the groups with low and high levels of ChR2. The IPSC accommodation remained higher in the slices with the lower amounts of ChR2, which indicated that ChR2 rather than virus per se attenuated the IPSC accommodation. Furthermore, the second possibility was ruled out because the higher levels of ChR2 did not change the membrane or firing properties in SOM-INs.

The role of photocurrents was tested by varying irradiance. The irradiance threshold for obtaining photocurrents in SOM-INs and IPSCs in PNs was same between the high- and low-ChR2 groups. Increasing irradiance increased photocurrents in both groups but the mean photocurrent obtained in the high ChR2 group with the weakest stimulation significantly exceeded those in the low ChR2 groups at all levels of stimulation. However, there was an overlap between the groups in photocurrents elicited in individual neurons [Fig. 2(h)].

The IPSCs in PNs also increased with irradiance, indicating increases in the number of recruited SOM-INs. Means IPSCs were comparable between the low ChR2 group at the higher irradiances and the high ChR2 group at the lowest irradiance, suggesting the same numbers of recruited SOM-INs under these conditions, despite the difference in the mean photocurrents. Increasing irradiance did not attenuate IPSC accommodation, suggesting the accommodation was not affected by the number of recruited SOM-INs, the amounts of GABA released in the slice, or the moderate changes in photocurrents with irradiance.

Because the mean photocurrent obtained in the high ChR2 group with the weakest stimulation exceeded the photocurrents in the low ChR2 group by several folds regardless the level of stimulation [Fig. 2(h)], a counteracting effect of the large photocurrents on inhibition of presynaptic GABA release machinery remains a plausible explanation for the attenuated IPSC depression. The GABA_BR signaling suppresses neurotransmitter release by inhibiting the adenylate cyclase and voltage-gated calcium channels at presynaptic terminals.¹⁶ Given that ChR2 conducts Ca²⁺,²² high photocurrents can provide a sufficient Ca²⁺ influx to over-ride the effect of inhibition of the voltage-gated calcium channels.

A prolonged (>80 days) viral expression of ChR2-YFP after injecting 3×10^9 viral particles in a single site has been reported to alter neuronal morphology in the cortical neurons.¹⁰ Although in our study the maximal amounts of AAV were 6 times lower and the incubation was below 45 days, a possibility remains that excessive levels of ChR2 in the plasma membrane interfere with normal assembly of the membrane-bound components of the second messenger signaling pathways and thereby making presynaptic terminals refractory to certain forms of neuromodulation. While in the high ChR2 group, we observed a small fraction of SOM-INs with a somatic accumulation of ChR2-YFP and unhealthy plasma membrane, the majority of SOM-INs appeared healthy and had the membrane and firing properties comparable to those in the low ChR2 group, despite the evidence that ChR2 can alter membrane capacitance.¹¹

Our findings do not imply that overexpression of ChR2 overrides all the presynaptic inhibitory mechanisms of neurotransmitter release. For example, activation of the dopamine receptor 2 in PV-INs and SOM-INs in the basolateral amygdala transduced with 5×10^8 viral particles of the identical virus per

hemisphere, which corresponds to the high amounts of virus in the present study, significantly attenuated blue light-induced GABA release from both types of interneurons.³ The main implication of our observation is that using ChR2 as a probe for synaptic plasticity carries a risk of interfering with the plasticity per se; however, such artifacts can be minimized by decreasing the amounts of ChR2 expression.

Disclosures

Authors declare no conflict of interest.

Acknowledgments

The study was supported by National Institutes of Health (NIH) Award No. MH112093.

References

1. L. Petreanu et al., "Channelrhodopsin-2-assisted circuit mapping of long-range callosal projections," *Nat. Neurosci.* **10**(5), 663–668 (2007).
2. C. K. Pfeffer et al., "Inhibition of inhibition in visual cortex: the logic of connections between molecularly distinct interneurons," *Nat. Neurosci.* **16**(8), 1068–1076 (2013).
3. H. Y. Chu et al., "Target-specific suppression of GABA release from parvalbumin interneurons in the basolateral amygdala by dopamine," *J. Neurosci.* **32**(42), 14815–14820 (2012).
4. J. H. Cho, K. Deisseroth, and V. Y. Bolshakov, "Synaptic encoding of fear extinction in mPFC-amygdala circuits," *Neuron* **80**(6), 1491–1507 (2013).
5. W. Ito, A. Erisir, and A. Morozov, "Observation of distressed conspecific as a model of emotional trauma generates silent synapses in the prefrontal-amygdala pathway and enhances fear learning, but ketamine abolishes those effects," *Neuropsychopharmacology* **40**(11), 2536–2545 (2015).
6. L. Liu, W. Ito, and A. Morozov, "GABA_B receptor mediates opposing adaptations of GABA release from two types of prefrontal interneurons after observational fear," *Neuropsychopharmacology* **42**(6), 1272–1283 (2017).
7. J. Mukai et al., "Molecular substrates of altered axonal growth and brain connectivity in a mouse model of schizophrenia," *Neuron* **86**(3), 680–695 (2015).
8. K. Kolodziejczyk and L. A. Raymond, "Differential changes in thalamic and cortical excitatory synapses onto striatal spiny projection neurons in a Huntington disease mouse model," *Neurobiol. Dis.* **86**, 62–74 (2016).
9. F. Zhang et al., "Multimodal fast optical interrogation of neural circuitry," *Nature* **446**(7136), 633–639 (2007).
10. T. Miyashita et al., "Long-term channelrhodopsin-2 (ChR2) expression can induce abnormal axonal morphology and targeting in cerebral cortex," *Front. Neural Circuits* **7**, 8 (2013).
11. D. Zimmermann et al., "Effects on capacitance by overexpression of membrane proteins," *Biochem. Biophys. Res. Commun.* **369**(4), 1022–1026 (2008).
12. Y. P. Zhang and T. G. Oertner, "Optical induction of synaptic plasticity using a light-sensitive channel," *Nat. Methods* **4**(2), 139–141 (2007).
13. S. L. Jackman et al., "Achieving high-frequency optical control of synaptic transmission," *J. Neurosci.* **34**(22), 7704–7714 (2014).
14. J. V. Raimondo et al., "Optogenetic silencing strategies differ in their effects on inhibitory synaptic transmission," *Nat. Neurosci.* **15**(8), 1102–1104 (2012).
15. M. Mahn et al., "Biophysical constraints of optogenetic inhibition at presynaptic terminals," *Nat. Neurosci.* **19**(4), 554–556 (2016).
16. M. Gassmann and B. Bettler, "Regulation of neuronal GABA(B) receptor functions by subunit composition," *Nat. Rev. Neurosci.* **13**(6), 380–394 (2012).
17. E. Perez-Garci et al., "The GABA_B1b isoform mediates long-lasting inhibition of dendritic Ca²⁺ spikes in layer 5 somatosensory pyramidal neurons," *Neuron* **50**(4), 603–616 (2006).
18. C. H. Davies and G. L. Collingridge, "The physiological regulation of synaptic inhibition by GABA_B autoreceptors in rat hippocampus," *J. Physiol.* **472**, 245–265 (1993).

19. A. Fukuda, I. Mody, and D. A. Prince, "Differential ontogenesis of presynaptic and postsynaptic GABA_B inhibition in rat somatosensory cortex," *J. Neurophysiol.* **70**(1), 448–452 (1993).
20. M. Kobayashi et al., "Kinetics of GABA_B autoreceptor-mediated suppression of GABA release in rat insular cortex," *J. Neurophysiol.* **107**(5), 1431–1442 (2012).
21. H. Taniguchi et al., "A resource of Cre driver lines for genetic targeting of GABAergic neurons in cerebral cortex," *Neuron* **71**(6), 995–1013 (2011).
22. G. Nagel et al., "Channelrhodopsin-2, a directly light-gated cation-selective membrane channel," *Proc. Natl. Acad. Sci. U. S. A.* **100**(24), 13940–13945 (2003).

Biographies for the authors are not available.